UCRL- 93301
PREPRINT



# CALCULATION OF AXIAL ELECTRON TEMPERATURE VARIATIONS IN TANDEM MIRRORS AT MODERATE COLLISIONALITY

T. D. Rognlien

This paper was prepared for submittal to
NUCLEAR FUSION

August 29, 1985

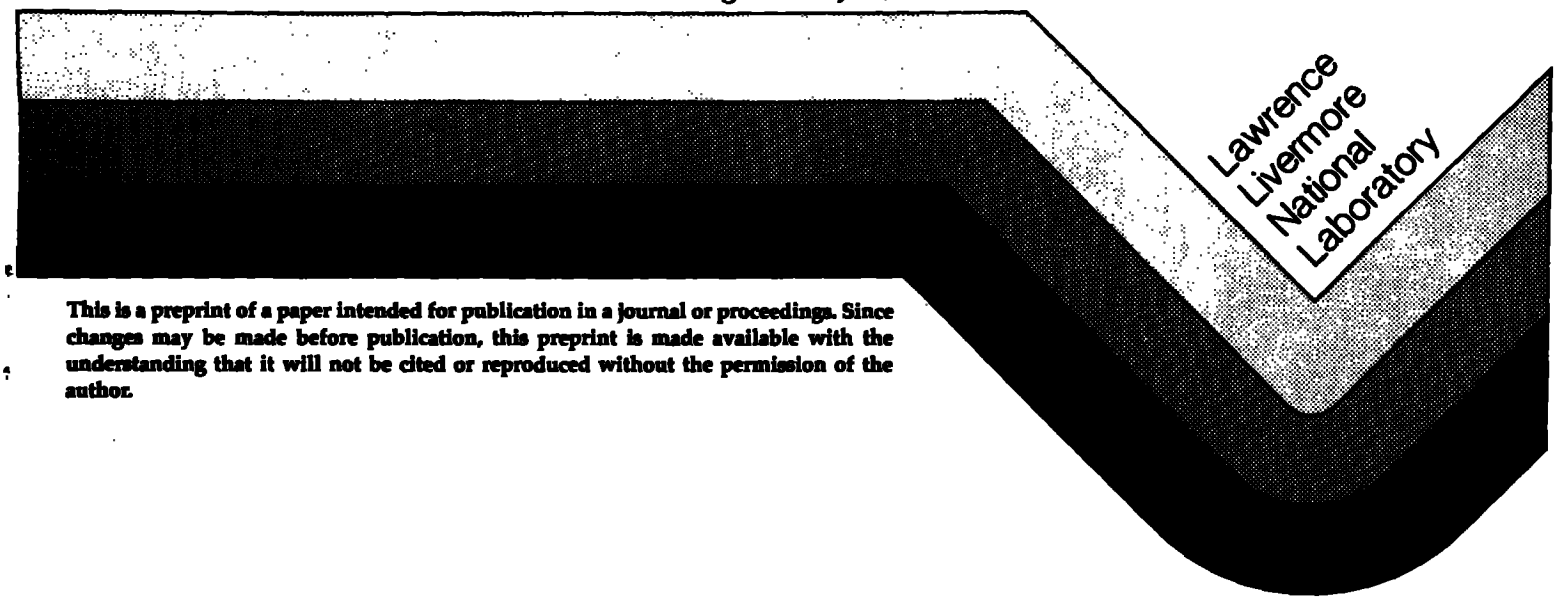

# CALCULATION OF AXIAL ELECTRON TEMPERATURE VARIATIONS IN TANDEM MIRRORS AT MODERATE COLLISIONALITY

T. D. Rognlien
Lawrence Livermore National Laboratory, University of California
Livermore, CA 94550

## ABSTRACT

A Monte Carlo test particle code is used to calculate the temperature difference between the central cell and end cell of a tandem mirror. The electron power input is through drag of hot ions in the end cell. It is found that the temperature difference increases as the mean free path becomes comparable to the system length. At long mean free paths, the temperature difference agrees with a previous analytical model. The calculation explains the temperature variation measured in the TMX experiment.

## I. INTRODUCTION

The understanding of electron heat transport along magnetic field lines is important for open-ended systems, such as magnetic mirrors, where field lines strike material surfaces or where thermal isolation of different energy groups is desired [1]. The two descriptions of this process are the short mean-free-path conduction model given by Spitzer [2] and the long mean-free-path model of Cohen et al. [3]. The latter description is generally valid for high-temperature fusion-oriented devices.

We shall show that finite mean-free-path effects can cause significant departures from the theory of Ref. [3] when the mean free path, $\lambda_c$, is a few times the device length, $L_d$. The calculation is performed using a Monte Carlo test particle code [4]. To be specific, we consider parameters relevant to the tandem mirror experiment TMX [5] where measured differences between the electron temperature in the central cell and end cell of roughly 2 indicates partial thermal isolation. This classical calculation does not invoke a thermal barrier [1] between the central cell and the end cell. The results should be relevant to other low temperature tandem mirrors such as Phaedrus [6] and GAMMA-6 [7].

The results show an enhanced isolation or reduced thermal transport as the plasma density is increased. Such an effect occurs because the heating power from electron drag in the end cell scales as density squared whereas the power loss by transport to the central cell begins to scale linearly with density, n, at high density. For $\lambda_c \gg L_d$, Ref. [3] predicts the energy loss scales as $n^2$, yielding a temperature difference independent of density.

The plan of the paper is as follows. In Sec. II the geometry and numerical model are presented. The numerical results are given in Sec. III, and an interpretation of the results is presented in Sec. IV.

## II. GEOMETRY AND NUMERICAL MODEL

### A. Axial Profiles

We consider a simple tandem mirror magnetic field configuration of the type found in the TMX experiment [5]. Figure 1 shows the axial profiles where we focus on variations in the end cell. There the ion density is made up mostly of hot neutral beam injected ions whose axial profile is taken as

$$n_{ih}(s) = n_{ho} \exp\left[-(s - s_e)^2/L_p^2\right] \tag{1}$$

where $s = s_e$ corresponds to the midplane of the end cell. The mean hot ion energy is $E_{ih}$. The central cell ions have a lower energy of $3\,T_{ic}/2$ and are confined by the electrostatic potential of the end cell. Their density has the form

$$n_{ic}(s) = n_{co} \exp\left[-e\Phi(s)/T_{ic}\right] \tag{2}$$

for $s < s_e$, and $n_{ic} = n_{ic}(s_e)$ for $s > s_e$. Here $\Phi(s)$ is the electrostatic potential.

The electron density profile is determined by quasineutrality, $n_e(s) = n_{ih}(s) + n_{ic}(s)$. The potential is found from the inertialess electron pressure balance equation

$$\frac{d}{ds} e\Phi = \frac{1}{n_e} \frac{d}{ds} n_e T_{\parallel} + \frac{T_{\perp} - T_{\parallel}}{B} \frac{dB}{ds} \qquad (3)$$

where B is the magnetic field strength. The effective electron temperatures are defined in terms of the corresponding mean parallel and perpendicular energies, i.e., $T_{\parallel} \equiv 2E_{\parallel}$ and $T_{\perp} \equiv E_{\perp}$. Thus, Eq. (3) is not restricted to Maxwellian distribution. Given $T_{\parallel,\perp}(s)$, one can use Eqs. (1)-(3) to find $n_e(s)$ and $\Phi(s)$.

## B. Evolution of the Test Electrons

The determination of $T_{\parallel,\perp}(s)$ in the end cell from test electrons is the central goal of our calculations. An iterative procedure is used where initial guesses for density and temperature profiles are updated by test particle data.

The electron source is assumed to be in the central cell, and the electrons there are taken as a Maxwellian with temperature $T_{ec}$. Thus, the test electrons are injected in the central cell as a right-going Maxwellian distribution at the left-hand boundary (see Fig. 1). The temperature $T_{ec}$ is assumed given and fixed for all iterations. In a real device, most electrons escape through the left-hand mirror back into the central cell because of the high potential at the right-hand mirror. For simplicity, we reflect all electrons at the right-hand mirror. We thus neglect the influence of the loss boundary for escape out of the device. However, the dominate power loss for end cell electrons is escape to and capture in the cooler central cell. Each escaping electron is replaced by a source electron to maintain zero current flow.

The axial orbits of the test electrons are followed in the plug region for small time steps using conservation of magnetic moment and total energy, together with $ds/dt = v_{||}$, where $v_{||}$ is the velocity along s. At each time step, the electrons are also scattered in velocity space by Coulomb collisions using a Monte Carlo technique [4]. The scattering coefficients depend on the local density and temperture of the Maxwellian "background" species doing the scattering [2]. The ion species are fixed for all iterations. For the first iteration, the temperature of the "background" electrons, $T_{eb}$, is taken from assumed profiles for parallel and perpendicular energy, $E_{||}$ and $E_{\perp}$.

$$T_{eb}(s) = 2\ [E_{||}(s) + E_{\perp}(s)]/3 \tag{4}$$

For simplicity, we let $E_{||} = E_{\perp} = 3T(s)/2$ on the first iteration.

At the end of an iteration, new profiles for $E_{||,\perp}(s)$ are available from the test electrons. However, we do not update the background energy profiles to have the same mean energy as the test electrons but instead choose the profile which gives no energy transfer between the background and test electrons. This distinction arises because the test electrons are composed of trapped and passing distributions at different temperatures rather than a single Maxwellian distribution. Consequently, there is a non-physical power transfer, $P_{bt}$, between the background electrons and the test electrons if one uses Eq. (4) directly with a single "background" Maxwellian. This power can be comparable to the actual power to the electrons, $P_D$, from the hot ions via drag where

$$P_D = A_m \int_{-\infty}^{\infty} ds\ \frac{n_{ih}(s)\ E_{ih}}{\tau_d}\ \frac{B(s_e)}{B(s)} \quad . \tag{5}$$

Here $A_m$ is the area of a flux tube at $s = s_e$, B(s) is the magnetic field strength, and $n_e\tau_d = 4.4 \times 10^7 T_e^{3/2}$ [$cm^{-3}s$] for $T_e$ in eV. It is the localized power from the hot ions which results in the end-cell electron energy being higher than in the central cell. The non-physical power transfer can be numerically measured by calculating the local power transferred from the background electrons to the test electrons, given by

$$P_{bt}(s) = \frac{m_e n_e(s)}{2t_t} \sum_i \left(2v_i \langle \Delta v_{\parallel} \rangle_i + \langle \Delta v_{\parallel}^2 \rangle_i + \langle \Delta v_{\perp}^2 \rangle_i\right) \Delta t_i \qquad (6)$$

Here the indice i runs over all the time steps, $\Delta t_i$, of the particle associated with the spatial grid cell at s, $v_i$ is the particle velocity, $t_t = \Sigma_i \Delta t_i$, $m_e$ is the electron mass, and the scattering coefficients with the angle brackets are given elsewhere [2].

To reduce $P_{bt}$ to zero, we calculate the effect local temperature difference, $\Delta T_e$, between the test electrons and the background electrons using the formula for power transfer between two electron species [2]. Specifically,

$$\Delta T_e(s) = \tau_{eq} \frac{dT_e}{dt} \approx \frac{2}{3} \tau_{eq} \frac{P_{bt}}{n_e(s)} \qquad (7)$$

where $\tau_{eq} \approx 3.2 \times 10^4 \, T_e^{3/2}(eV)/n_e(cm^{-3})$ [s] for $\Delta T_e << T_e$. After calculating $\Delta T_e$ at the end of one iteration, the temperature used in the Coulomb scatter coefficients for the next iteration is a modification of Eq. (3)

$$T_{eb} = 2(E_{\parallel} + E_{\perp})/3 + \Delta T_e \quad . \qquad (8)$$

After the second iteration, this procedure reduces the volume-integrated non-physical power transfer to a sufficiently low level that the physical hot

ion drag power is an order of magnitude larger. A steady state is reached when $T_{\parallel,\perp}(s)$ and $\Delta T_e(s)$ stop changing, typically four to five iterations.

## III. NUMERICAL RESULTS

To illustrate the effect of finite mean free path on the end-cell-to-central-cell temperature ratio, we use parameters associated with the TMX tandem mirror experiment [5]. The base-case densities used to model the experiment are $n_{ho} = 1.5 \times 10^{13}$ cm$^{-3}$ and $n_{co} = 2.5 \times 10^{12}$cm$^{-3}$; we shall keep the ratio of the end-cell-to-central-cell density fixed at 6 but vary the densities to show scaling. Other parameters are the hot ion scale length $L_p = 15$ cm, $E_{ih} = 13$ keV, and $T_{ic} = 50$ eV. The center cell electron temperature is fixed at 40 eV.

The plasma density falls to a low value before reaching the right-hand mirror throat at $s = s_e + 57$ cm (see Fig. 1) because the ion density is only composed of escaping ions there. Consequently, the number of test electrons reaching the throat is small and the statistical fluctuation in the calculated energy can be large. We thus reflect the electrons at $s = s_e + 40$ cm where the density is a factor $\sim$50 lower than the midplane value. The collisional processes which would occur between $s = s_e + 40$ cm and the mirror throat are negligibly small owing to the low density.

The steady-state profiles obtained for $T_{\parallel,\perp}(s)$ and $\Phi(s)$ after 5 iterations are shown in Fig. 2 for the base case densities. Note that there is a slight anisotropy with $T_\perp > T_\parallel$. This occurs because in the magnetic well the colder passing electrons from the central cell contribute more to the

parallel than perpendicular energy. Also, electrons with mostly perpendicular energy are better confined and less likely to be exchanged for central-cell electrons.

The contour plot of the electron distribution function f in Fig. 3 illustrates the points just discussed. The plot corresponds to the end-cell midplane, $s = s_e$. The separatrix between trapped and passing electrons shows the cooler passing central cell electron population with more closely spaced contours; each contour corresponds to a decrease in the value of f by a factor of 1.39. The trapped and passing distributions are closely fit by Maxwellians at temperature $T_{ep}(0)$ and $T_{ec}$, respectively.

In Fig. 4, we show the value of $\Delta T_e(s)$ as calculated from Eq. (7). For the parameters used, the omission of $\Delta T_e$ in Eq. (8) would result in a non-physical power transfer to the background electrons comparable to the drag power input.

The effect of varying the density on $T_{ep}(0)$ and $\Phi(0)$ is shown in Fig. 5; the ratio $n_{ho}/n_{co} = 6$ for all cases. The fact that both increase with density is the principle result of this study. Shown for comparison is the value of $T_{ep}(0)$ predicted from the long mean-free-path theory [3], which is independent of density. This value can be calculated from Eqs. (31) and (32) of Ref. [3] or estimated from Fig. 7 of that paper. The input power parameter, $\hat{P}$, scales inversely with $T_{ep}$ and directly with ion energy; bounce averaging reduces $\hat{P}$ because the drag power density is proportional to $n^2$. For the parameters here, $\hat{p} \approx 140$, and extrapolating from Fig. 7 of Ref. [3] for $n_b/n_p = 1/6$ gives $T_{ec}/T_{ep} \sim 0.65$, or $T_{ep} = 62$ eV. The corresponding potential is $\Phi = 98$ V. Note that the numerical results appear

to be approaching these values at low density. For the TMX experiment [5], $n_p \approx 1.5 \times 10^{13}$ cm$^{-3}$, and $T_{ec} \approx 49$ eV, and $T_{ep} \approx 87$ eV for a ratio $T_{ec}/T_{ep} = 1.8$. Figure 5 yields the ratio $T_{ep}/T_{ec} \approx 2.1$. Thus, the temperature difference observed in TMX is consistent with Coulomb collisions alone in the absence of a thermal barrier.

## IV. DISCUSSION AND SUMMARY

The main result of this paper is that the temperature difference between a trapped population of electrons and a passing population becomes a function of density at moderate mean free paths ($\lambda_c \lesssim 3\ L_d$) resulting in an increase in the temperature difference. For the problem we have considered, the device length, $L_d$, is given by the length of the end cell, ∿100 cm. The mean free path for electron-electron collisions is

$$\lambda_c \approx 5 \times 10^{11}\ T_e^2/n_e\ [\text{cm}] \tag{9}$$

for $T_e$ in eV and $n_e$ in cm$^{-3}$. For the low density point in Fig. 5, we find $\lambda_c/L_d \approx 6$, and the theoretical prediction of Ref. [3] is a good fit. For the density of TMX, $n_p \approx 1.5 \times 10^{13}$ and $\lambda_c/L_d \approx 2$; there is then a significant departure of $T_{ep}$ from Ref. [3].

As the mean free path becomes shorter, the characteristics of the passing distribution can be significantly altered such that the portion returning to the central cell will have a mean energy part way between those of the trapped and passing distributions. Thus, deviations from Ref. [3] should be expected. On the other hand, it was shown previously [8] that for $\lambda_c/L_d \sim 1$, the Spitzer

thermal conductivity over estimates the thermal flux by a large factor. A better fit to this parameter regime was found to be the energy flux at the mirror throat calculated as though right going and left going particles have the temperature $T_{ec}$ and $T_{ep}$, respectively. This yields an energy flux given by [8]

$$Q = \frac{2n_c v_{tc} A_t}{\sqrt{\pi}} \frac{(T_{ep} - T_{ec})}{1 + (T_{ec}/T_{ep})^{1/2}} \tag{10}$$

where $v_{tc} = (2T_{ec}/m_e)^{1/2}$ and $A_t$ is the area at the mirror throat.

Equation (10) gives an upper bound on the amount of heat flux escaping into the central cell as the left going distribution will at most have a temperature $T_{ep}$, but generally less. Note that Eq. (10) scales as density whereas the energy transfer terms for $\lambda_c >> L_d$ scale as $n^2$ [see Eq. (29) of Ref. 3]. Thus, as the density is increased, the heat flow will be restricted by Eq. (10) as it is an upper bound. When Eq. (10) is set equal to the power input from drag, Eq. (5), we have a nonlinear equation for $T_{ep}$:

$$\frac{2n_c v_{tc}}{\sqrt{\pi} R_m} \frac{(T_{ep} - T_{ec})}{1 + (T_{ec}/T_{ep})^{1/2}} = \frac{n_{ho}^2 E_{hi}}{n_{ho} \tau_d} (\pi/2)^{1/2} L_p \tag{11}$$

The drag rate $\tau_d$ is evaluated using $T_{ep}$, and $R_m = A_m/A_t$ is the mirror ratio. The solution to this equation is plotted as a dotted line on Fig. 5. Because Eq. (10) is an upper bound on the heat flux, the dotted line for $T_{ep}$ is a lower bound. Thus, a least above $n_p \approx 4 \times 10^{13}$ cm$^{-3}$, the calculated value of $T_{ep}$ must be greater than the long mean-free-path value from Ref. [3]. The points lie significantly above the dotted line because the distribution returning to the central cell has a temperature less than $T_{ep}$.

We thus find the result that as one approaches a shorter mean-free-path plasma, the thermal isolation of the end cell improves. Such behavior is similar to that of the product of the density and particle confinement time, $n\tau_p$, which also increases as the mean free path becomes shorter [4].

## ACKNOWLEDGMENTS

The author gratefully acknowledges useful discussions with R. H. Cohen and D. P. Grubb. In a preliminary calculation R. H. Cohen has found that the theory of Ref. 3 is significantly affected by finite transit effects for TMX parameters.

This work was performed under the auspices of the U.S. Department of Energy by the Lawrence Livermore National Laboratory under contract number W-7405-ENG-48.

REFERENCES

1. Baldwin, D. E., and Logan, B. G., Phys. Rev. Lett. 43 (1979) 1318.

2. Spitzer, L., Jr., Physics of Fully Ionized Gases, Interscience, New York, (1967) Chap. 5.

3. Cohen, R. H., Bernstein, I. B., Dorning, J. J., and Rowlands, G., Nucl. Fusion 20 (1980) 1421.

4. Rognlien, T. D. and Cutler, R. A., Nucl. Fusion 20 (1980) 1003.

5. Grubb, D. P., Allen, S. L., Casper, T. A., Clauser, J. F., Coensgen, F. H., Cohen, R. H., Correll, D. L., Cummins, W. C., Davis, J. C., Drake, R. P., Foote, J. H., Futch, A. H., Goodman, R. K., Gryczkowski, G. E., Hooper, E. B. Jr., Hornady, R. S., Hunt, A. L., Karmendy, C. V., Nexsen, W. E., Pickles, W. L. Porter, G. D., Poulsen, P., Rognlien, T. D., Simonen, T. C., Slaughter, D. R., Coakley, P., Hallock, G. A., Strand, O. T., Phys. Fluids 26 (1983) 1987.

6. Hershkowitz, N., Breun, R. A., Brouchers, D., Callen, J. D., Chan, C., Conrad, J. R., Ferron, J., Golovato, S. N., Horne, S., Nelson, B., Peranich, L., Persing, H., Yujiri, L., McVey, B., Molvik, A., Smatlak, D., in Plasma Phys. and Controlled Nucl. Fusion Res. (Proc. 9th Int. Conf., Baltimore, 1982) Vol. I, IAEA, Vienna (1983) 553.

7. Inutake, M., Ishii, K., Itakura, A., Katanuma, I., Kawabe, T., Kiwamoto, Y., Muse, A., Miyoshi, S., Saito, T., Sausada, K., Tsubouchi, D., Yatsu, K., Aizawa, M., Kamimura, T., Itatani, R., Yasaka, Y., in Plasma Phys. and Controlled Nucl. Fusion Res. (Proc. 9th Int. Conf., Baltimore, 1982) Vol. I, IAEA, Vienna (1983) 544.

8. Khan, S. A. and Rognlien, T. D., Phys. Fluids 24 (1981) 1442.

FIGURE CAPTIONS

Fig. 1. Axial profiles at the end cell of a tandem mirror. The densities $n_{ic}$ and $n_{ih}$ correspond to those of cold and hot ions, respectively, and B is the magnetic field.

Fig. 2. Test electron data of perpendicular and parallel electron temperatures $T_\perp$ and $T_\parallel$, together with axial potential, $\Phi$, for the base case with $n_{ho} = 1.5 \times 10^{13}$ cm$^{-3}$ after 5 iterations.

Fig. 3. Electron distribution function at end-cell midplane ($s = s_e$) corresponding to Fig. 2. The passing distribution is below the separatrix line.

Fig. 4. Electron temperature increment calculated from Eq. (7) to obtain zero power transfer between test and background electrons for conditions of Fig. 2.

Fig. 5. Calculated end-cell electron temperature, $T_{ep}$, and potential, $\Phi$, at various end-cell densities for constant ratio $n_{ho}/n_{co} = 6$. The solid line is the long-mean-free path theory of Ref. 3 and the dotted line is the lower bound from Eq. (11).

T. D. Rognlien - Figure 1

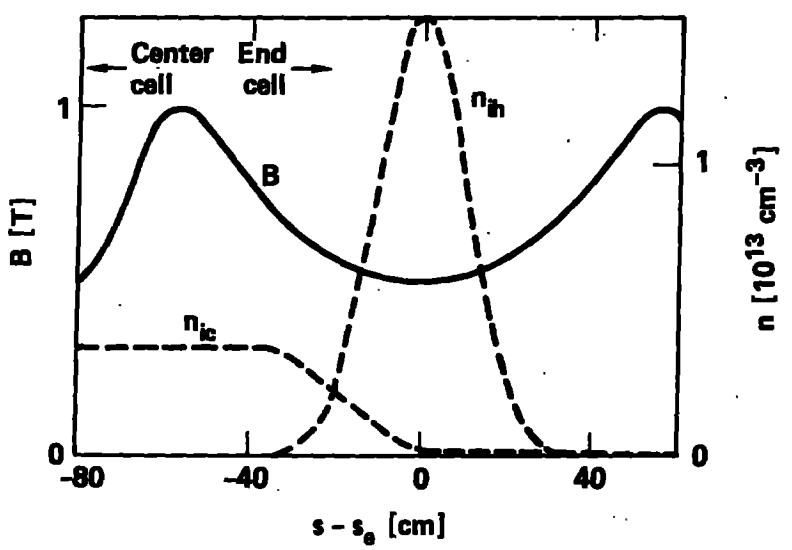

T. D. Rognlien - Figure 2

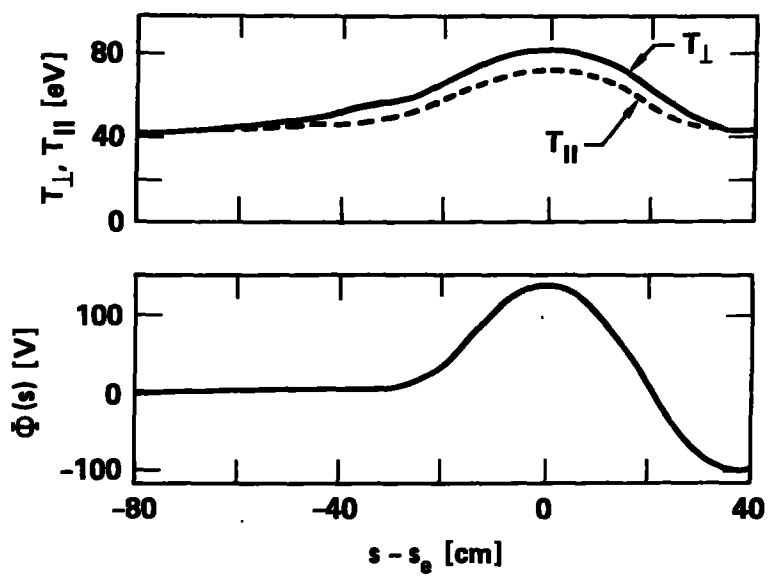

T. D. Rognlien - Figure 3

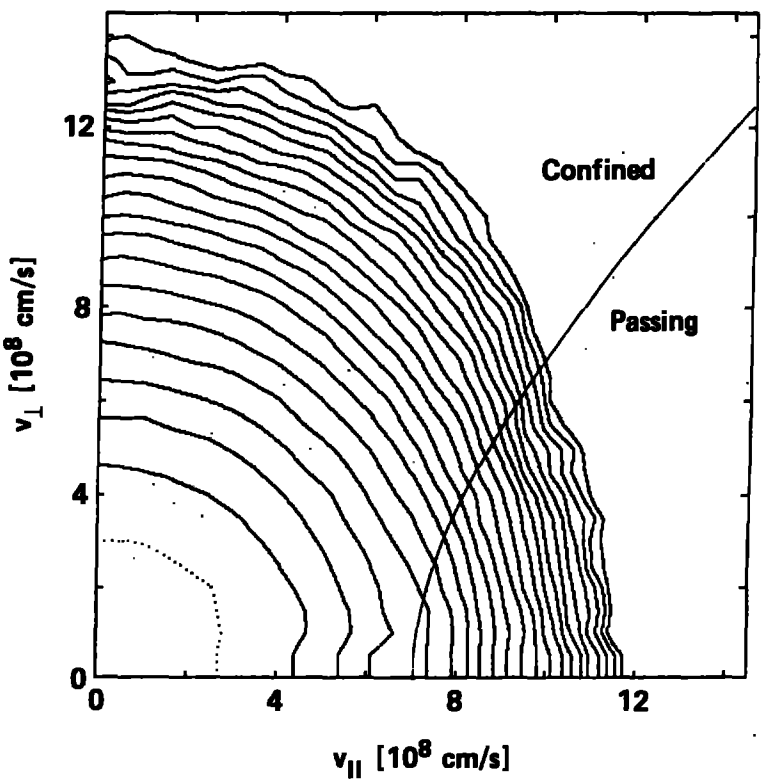

T. D. Rognlien - Figure 4

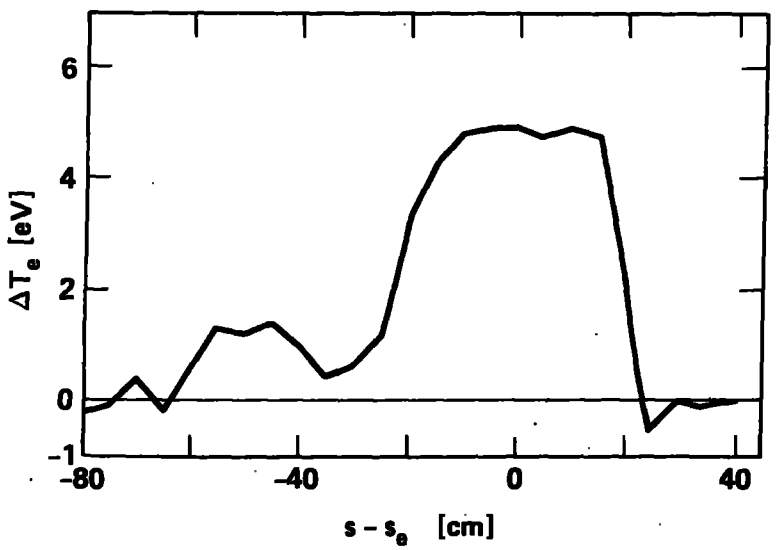

T. D. Rognlien - Figure 5